# Supporting Information

# Synthesis of $SiO_2$@$MnCo_2O_4$ core-shell nanorattles using layered double hydroxide precursors and studies on their peroxidase-like activity

Pankaj Rana and Pethaiyan Jeevanandam*
Department of Chemistry, Indian Institute of Technology Roorkee, Roorkee-247667, India
E-mail: jeevafcy@iitr.ac.in; Fax: +91-1332-273560; Tel: +91-1332-285444

**Characterization of $SiO_2$@MnCo-LDH precursors**

**Phase analysis**

The XRD patterns of $SiO_2$ and $SiO_2$@MnCo-LDH precursors are displayed in Figure S1. The XRD pattern of $SiO_2$ displays broad humps indicating its amorphous nature. The XRD pattern of MnCo-LDH displays (00*l*) basal reflections in the low 2θ region characteristic of layered double hydroxides.[1] The XRD peaks around 2θ = 11.6°, 23.7°, 33.2°, and 58.3° are assigned to (003), (006), (101), and (110) planes of MnCo-LDH. The XRD patterns of $SiO_2$@MnCo-LDH samples ($SiO_2$@MnCo-LDH-0.25, $SiO_2$@MnCo-LDH-0.5, and $SiO_2$@MnCo-LDH-1) show peaks around 2θ = 11.6°, 23.9°, 33.3°, and 58.2° attributed to the different crystal planes of MnCo-LDH. The interlayer spacing, estimated using (003) reflections of MnCo-LDH and $SiO_2$@MnCo-LDH samples, is about 7.6 Å.

**FT-IR analysis**

Figure S2 shows the FT-IR spectra of $SiO_2$, MnCo-LDH, and $SiO_2$@MnCo-LDH samples ($SiO_2$@MnCo-LDH-0.25, $SiO_2$@MnCo-LDH-0.5, and $SiO_2$@MnCo-LDH-1). Table S1 gives the summary of IR bands and assignment for MnCo-LDH and $SiO_2$@MnCo-LDH samples. The IR spectrum of $SiO_2$ shows characteristic peaks at about 1100 $cm^{-1}$ and 795 $cm^{-1}$ due to asymmetric and symmetric stretching vibrations of Si-O-Si, respectively. The IR bands observed at about 958 $cm^{-1}$ and 469 $cm^{-1}$ are assigned to stretching vibration of Si-OH and bending vibration of Si-O-Si, respectively.[2] The IR spectrum of MnCo-LDH shows bands around 2217 $cm^{-1}$ and 1382 $cm^{-1}$ due to $OCN^-$ and $NO_3^-$, respectively. The band observed at about 639 $cm^{-1}$ is ascribed to the stretching vibration of M-OH bond (M = Mn, Co) of MnCo-LDH. The IR spectra of all the $SiO_2$@MnCo-LDH precursors show characteristic bands of $SiO_2$ at 1107 $cm^{-1}$ and 476 $cm^{-1}$ due to υ-Si-O-Si and δ-Si-O-Si, respectively. The bands observed at about 2230 $cm^{-1}$ and 1388 $cm^{-1}$ are ascribed to the $OCN^-$ and $NO_3^-$ ions present in the interlayer galleries of MnCo-LDH.[3] The band observed at about 659 $cm^{-1}$ is ascribed to stretching vibration of the M-OH bond (M = Mn, Co) in the $SiO_2$@MnCo-LDH precursors.

**Thermal gravimetric analysis**

Figure S3 depicts the TGA curves of $SiO_2$, MnCo-LDH, and $SiO_2$@MnCo-LDH samples ($SiO_2$@MnCo-LDH-0.25, $SiO_2$@MnCo-LDH-0.5, and $SiO_2$@MnCo-LDH-1). Table S2 gives the summary of TGA results. The TGA curve of $SiO_2$ shows the first weight loss step (~5 %) observed between 30 °C and 160 °C which is ascribed to the loss of physisorbed water molecules. The second weight loss step (~ 7.2 %) in the temperature range 200 °C to 600 °C is due to the removal of surface hydroxyl groups of $SiO_2$.[2] The TGA curve of MnCo-LDH displays the first weight loss step of about 4.7 % below 145 °C which is ascribed to the loss of physisorbed water molecules. The second weight loss step of about 17.7 % between 145 °C and 350 °C is due to the decomposition of intercalated nitrate ($NO_3^-$) and isocyanate ($OCN^-$) anions present in MnCo-LDH.[3] The third weight loss step (~ 6.1 %) between 350 °C and 550 °C is attributed to the dehydroxylation of hydroxide layers of MnCo-LDH. The TGA curves of $SiO_2$@MnCo-LDH-0.25, $SiO_2$@MnCo-LDH-0.5, and $SiO_2$@MnCo-LDH-1 show the first weight loss step of about 7.0 %, 8.0 %, and, 4.2 %, respectively, between 30 °C and 160 °C ascribed to the loss of physisorbed $H_2O$ molecules. The second weight loss step of about 3.4 %, 5.2 %, and 12.8 %, respectively between 160 °C and 350 °C corresponds to decomposition of nitrate and isocyanate anions intercalated between the galleries of MnCo-LDH in $SiO_2$@MnCo-LDH samples. The final weight loss step of about 5.2 %, 3.2 %, and 6.2 % between 350 °C and 600 °C corresponds to decomposition of hydroxide layers of MnCo-LDH present on the surface of $SiO_2$ (spheres) in $SiO_2$@MnCo-LDH-0.25, $SiO_2$@MnCo-LDH-0.5, and $SiO_2$@MnCo-LDH-1, respectively.

## Morphological and elemental analyses

Figure S4(a-e) depicts the FESEM images of $SiO_2$, MnCo-LDH, and $SiO_2$@MnCo-LDH samples before calcination. Figure S4(a) shows spherical $SiO_2$ particles with an average diameter of 162.5 ± 14.5 nm. The FESEM image of MnCo-LDH (Figure S4(b)) displays thin nanosheets (particles with flake-like morphology). The FESEM images of $SiO_2$@MnCo-LDH samples (Figure S4(c-e)) display that the $SiO_2$ spheres are coated with MnCo-LDH nanosheets to form core-shell nanoparticles. Table S3 summarizes the elemental analysis data (EDXA results) for all the $SiO_2$@MnCo-LDH precursors. The EDXA results indicate uniform elemental composition of Si, Mn, Co, and O in all the $SiO_2$@MnCo-LDH precursors.

## Figures and Tables:

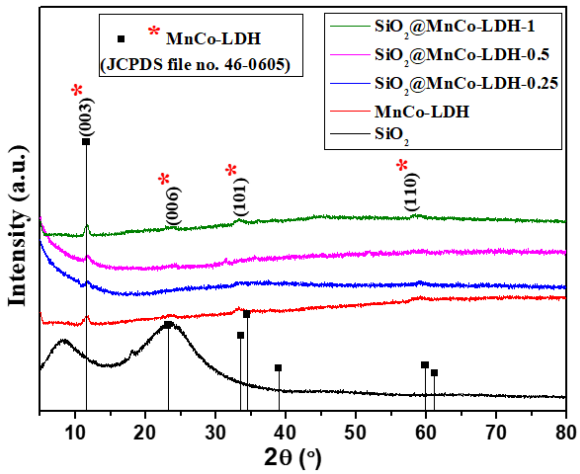


**Fig. S1** XRD patterns of $SiO_2$, MnCo-LDH, and $SiO_2$@MnCo-LDH precursors.

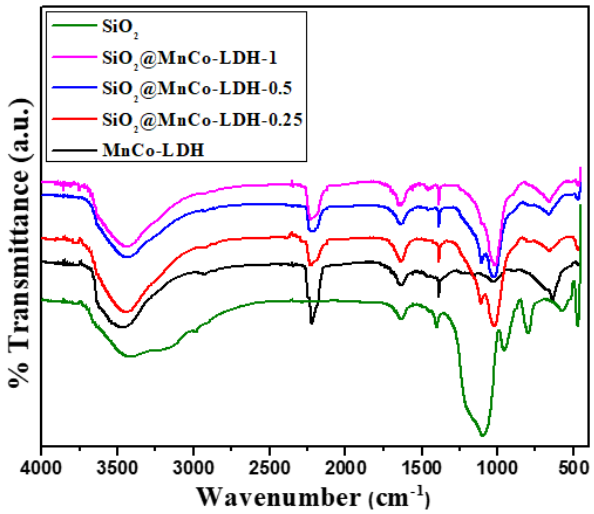


**Fig. S2** FT-IR spectra of $SiO_2$, MnCo-LDH, and $SiO_2$@MnCo-LDH samples.

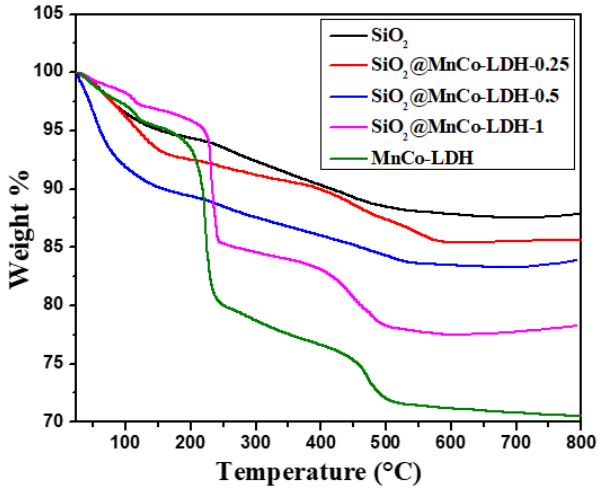


**Fig. S3** TGA curves of $SiO_2$, MnCo-LDH and $SiO_2$@MnCo-LDH samples.

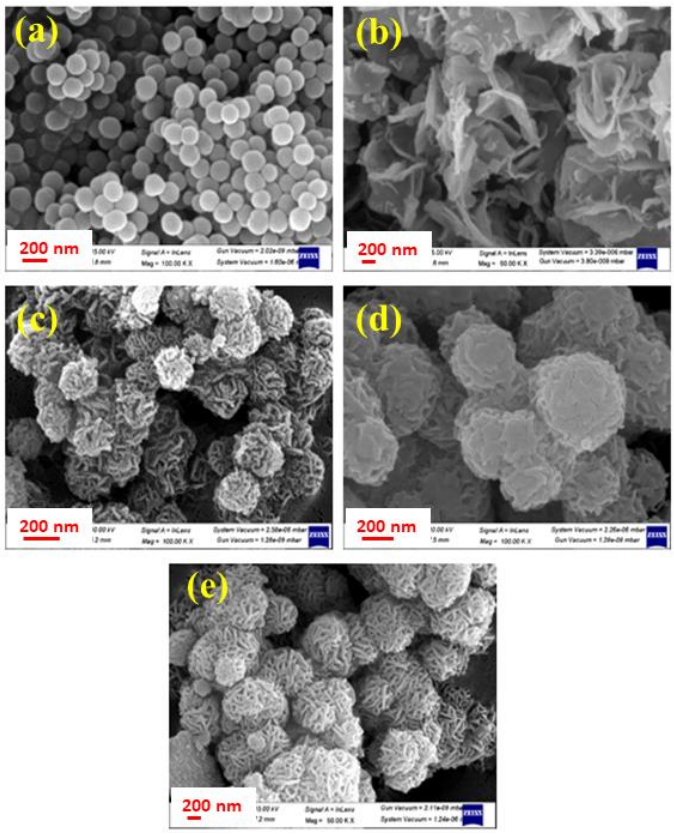


**Fig. S4** FE-SEM images of (a) $SiO_2$, (b) MnCo-LDH, (c) $SiO_2$@MnCo-LDH-0.25, (d) $SiO_2$@MnCo-LDH-0.5, and (e) $SiO_2$@MnCo-LDH-1.

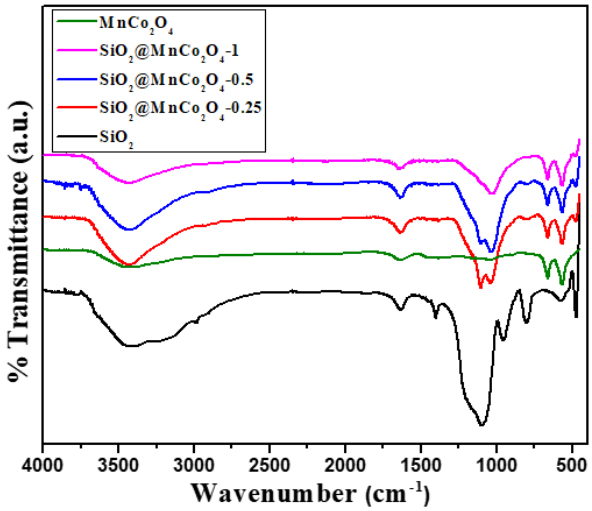


**Fig. S5** FT-IR spectra of $SiO_2$, $MnCo_2O_4$, and $SiO_2@MnCo_2O_4$ samples calcined at 500 ℃.

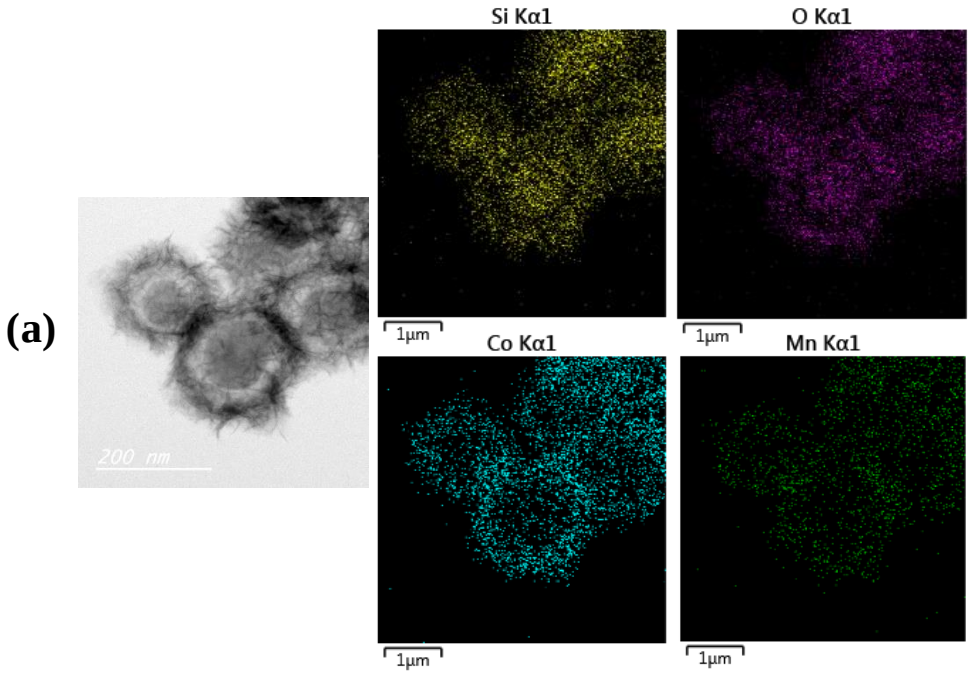

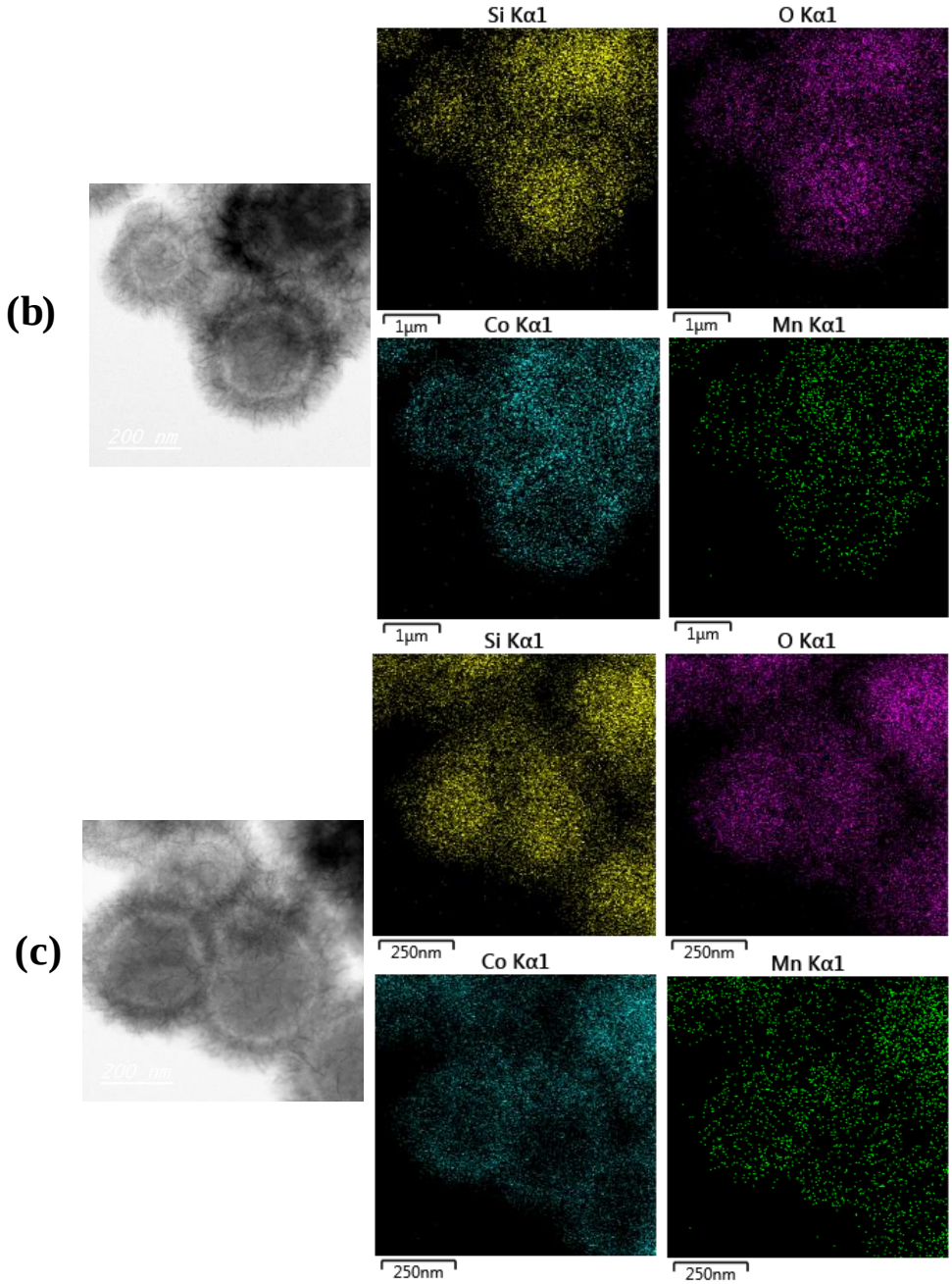


**Fig. S6** EDS mapping images of (a) $SiO_2$@$MnCo_2O_4$-0.25, (b) $SiO_2$@$MnCo_2O_4$-0.5 and (c) $SiO_2$@$MnCo_2O_4$-1 core-shell nanorattles.

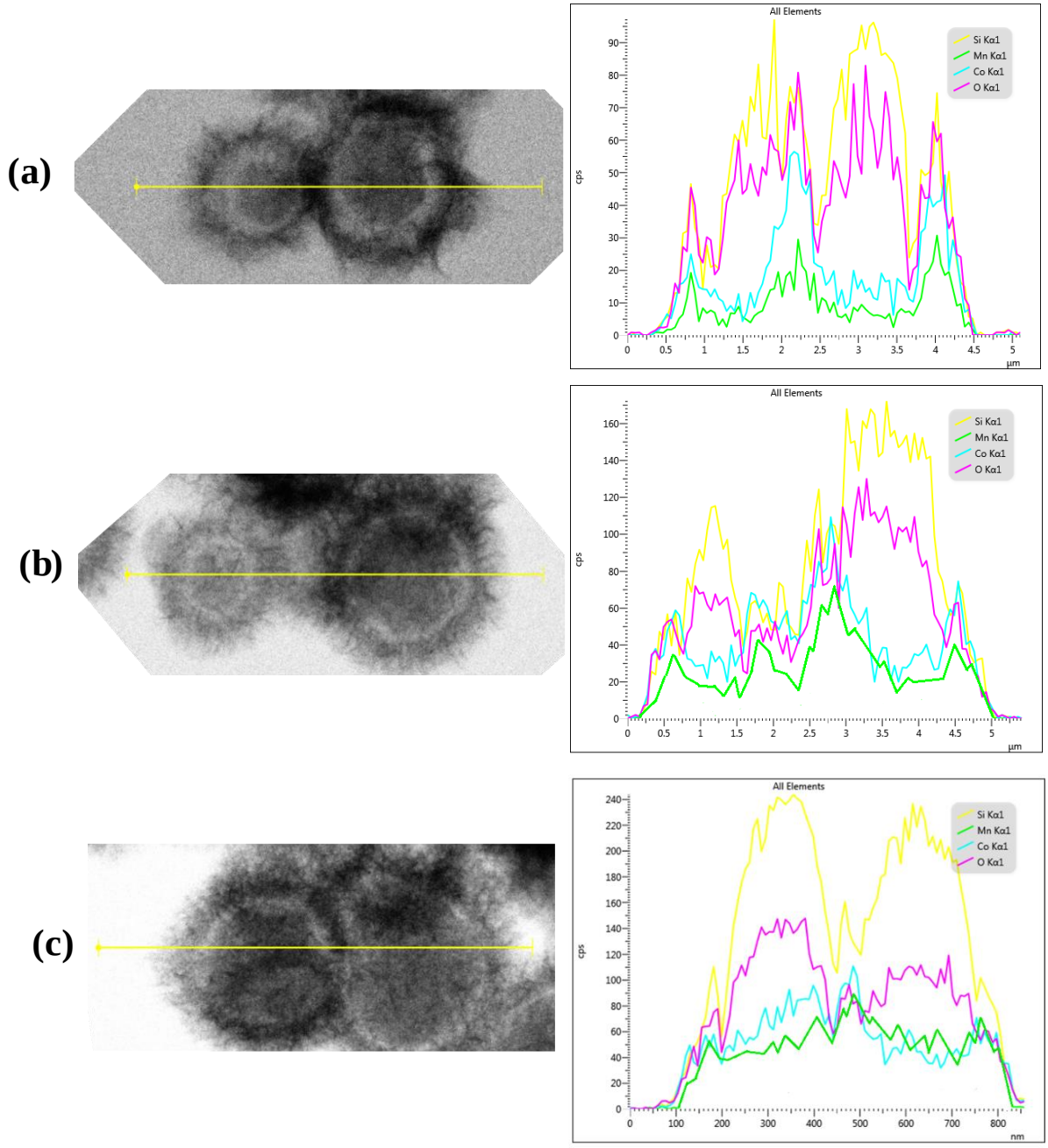


**Fig. S7** Linear scan EDS analysis data of (a) $SiO_2$@$MnCo_2O_4$-0.25, (b) $SiO_2$@$MnCo_2O_4$-0.5 and (c) $SiO_2$@$MnCo_2O_4$-1 core-shell nanorattles.

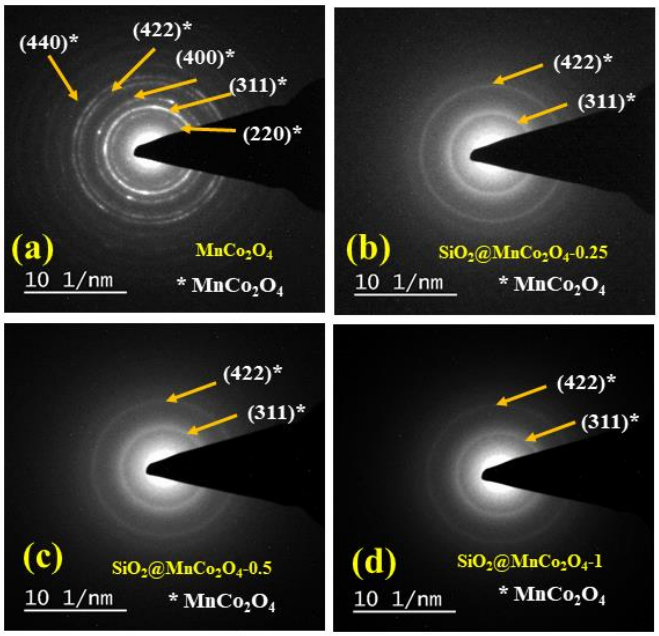


**Fig. S8** SAED patterns of (a) $MnCo_2O_4$, (b) $SiO_2@MnCo_2O_4$-0.25, (b) $SiO_2@MnCo_2O_4$-0.5 and (d) $SiO_2@MnCo_2O_4$-1 samples.

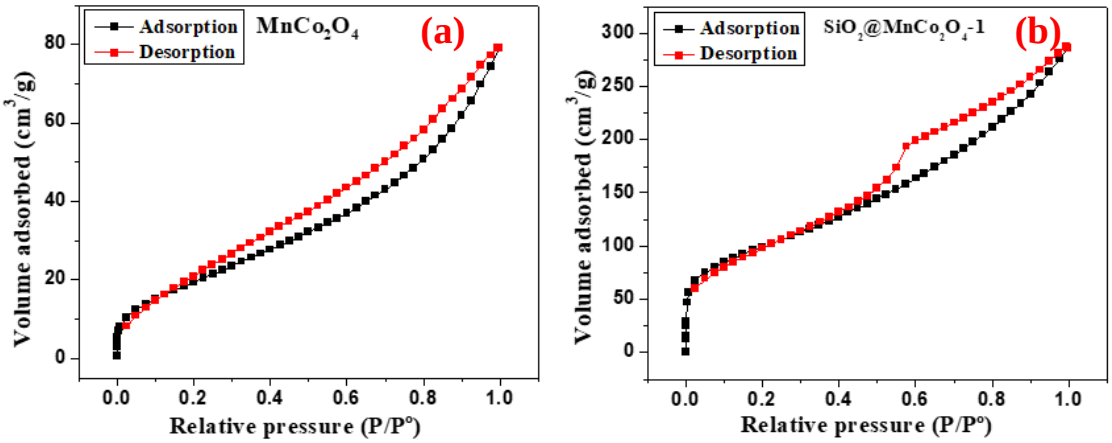


**Fig. S9** Adsorption-desorption isotherms of (a) $MnCo_2O_4$ NPs and (b) $SiO_2@MnCo_2O_4$-1 core-shell nanorattles.

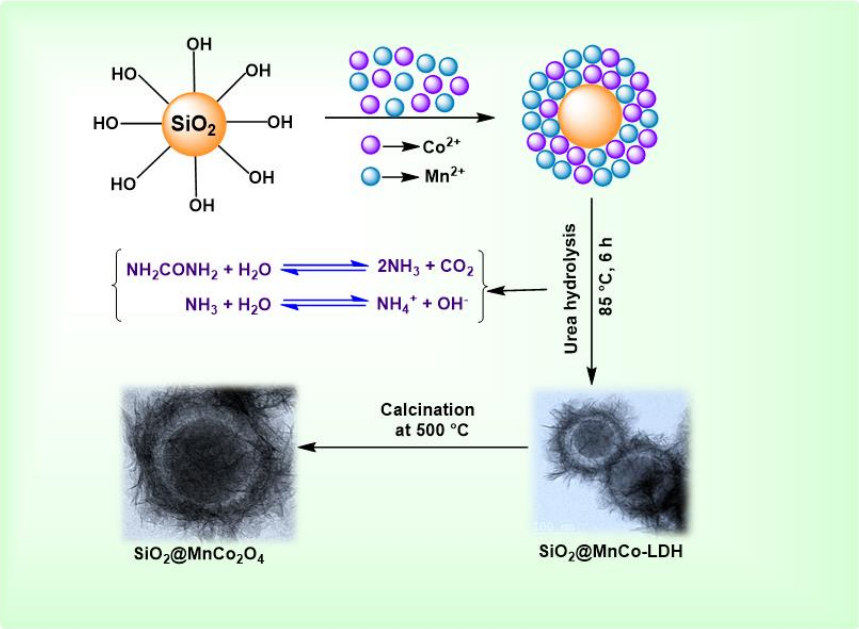


**Fig. S10** Proposed mechanism of formation of $SiO_2$@$MnCo_2O_4$ core-shell nanorattles.

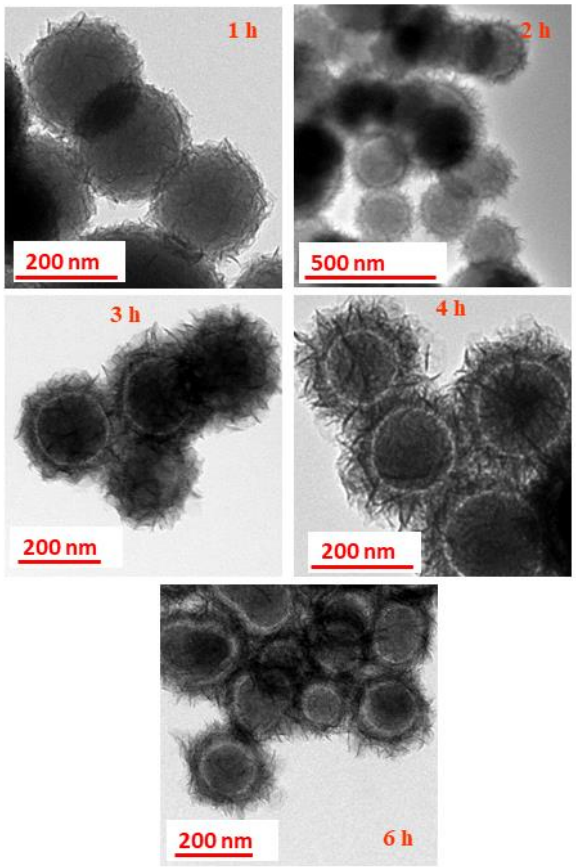


**Fig. S11** Time-dependent TEM images of $SiO_2$@MnCo-LDH-0.25.

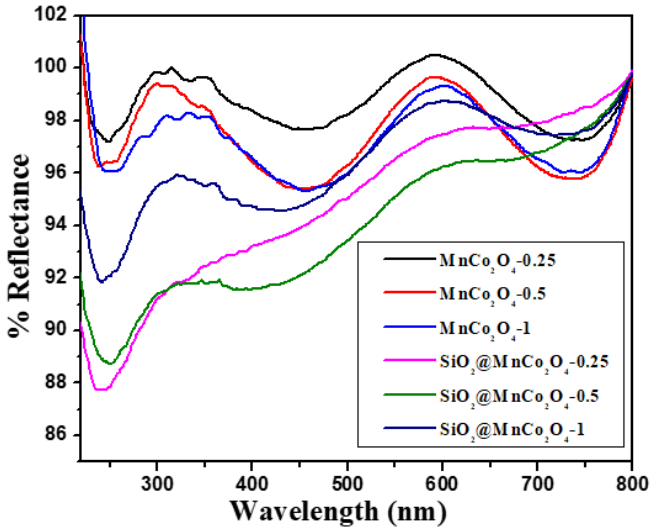


**Fig. S12** DRS spectra of $MnCo_2O_4$ NPs and $SiO_2@MnCo_2O_4$ core-shell nanorattles.

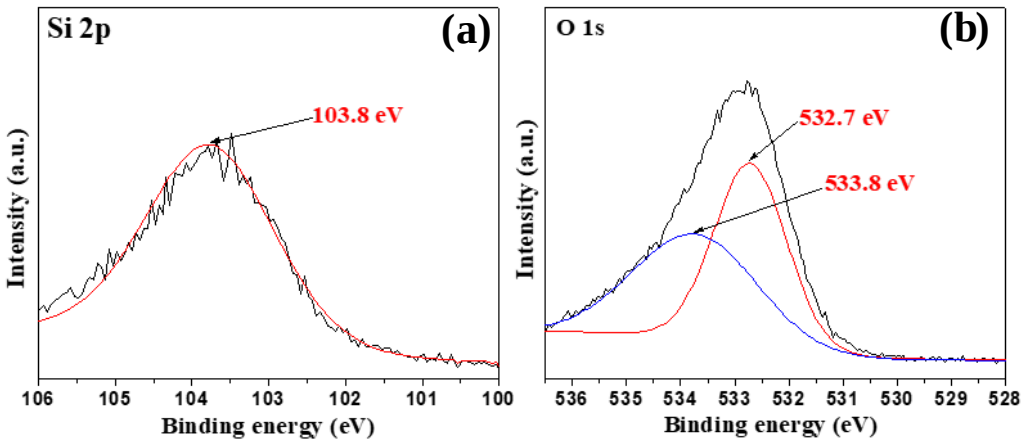


**Fig. S13** XPS spectrum of $SiO_2$: (a) Si 2p and (b) O 1s.

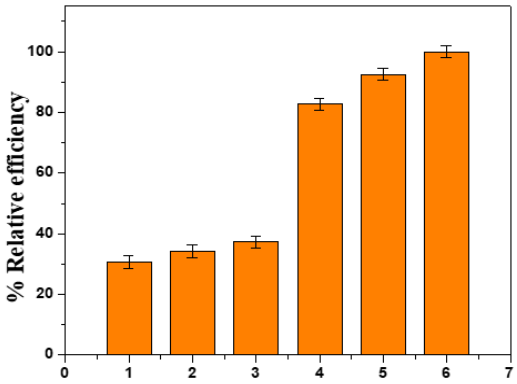


| Sl. No. | Sample code |
|---|---|
| 1 | $MnCo_2O_4$-0.25 |
| 2 | $MnCo_2O_4$-0.5 |
| 3 | $MnCo_2O_4$-1 |
| 4 | $SiO_2$@$MnCo_2O_4$-0.25 |
| 5 | $SiO_2$@$MnCo_2O_4$-0.5 |
| 6 | $SiO_2$@$MnCo_2O_4$-1 |

**Fig. S14** % Relative efficiency of $MnCo_2O_4$ NPs and $SiO_2$@$MnCo_2O_4$ core-shell nanorattles as catalyst during peroxidase-like activity.

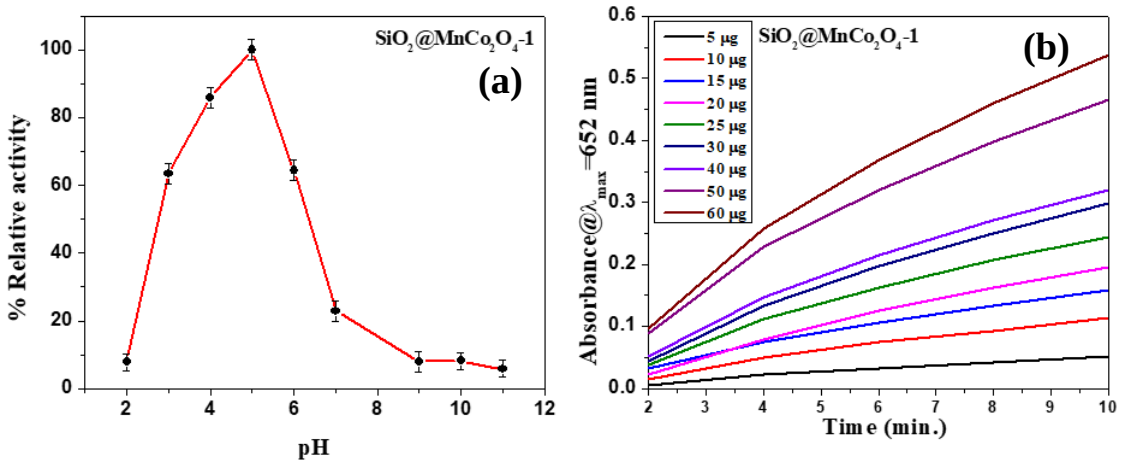


**Fig. S15** Effect of experimental conditions on peroxidase-like activity of $SiO_2$@$MnCo_2O_4$ core-shell nanorattles; (a) pH and (b) amount of catalyst dispersion.

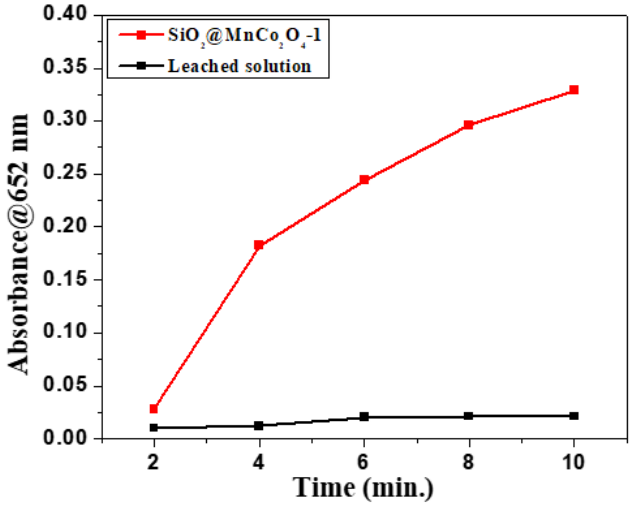


**Fig. S16:** Leaching test results during the peroxidase-like activity of $SiO_2$@$MnCo_2O_4$-1 core-shell nanorattles.

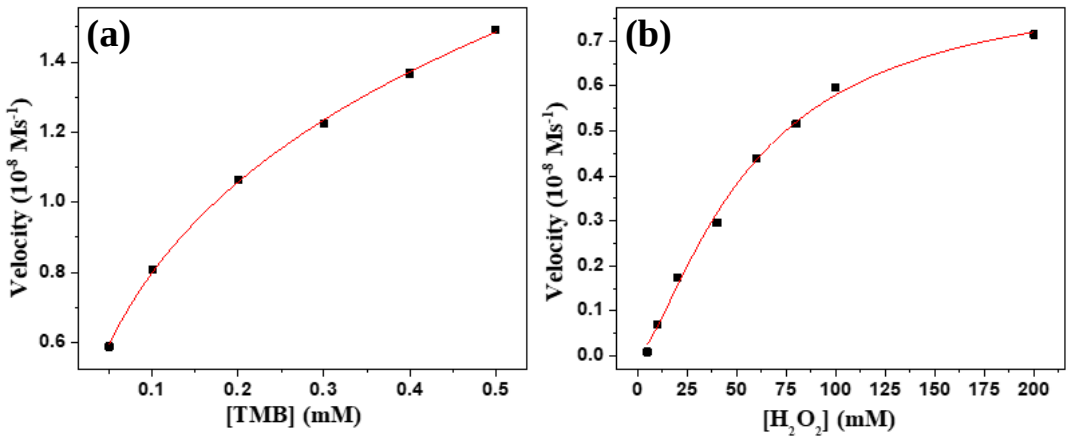


**Fig. S17** Steady-state kinetics results of $SiO_2$@$MnCo_2O_4$-1 core-shell nanorattles using different substrates during the peroxidase-like activity studies: (a) TMB and (b) $H_2O_2$.

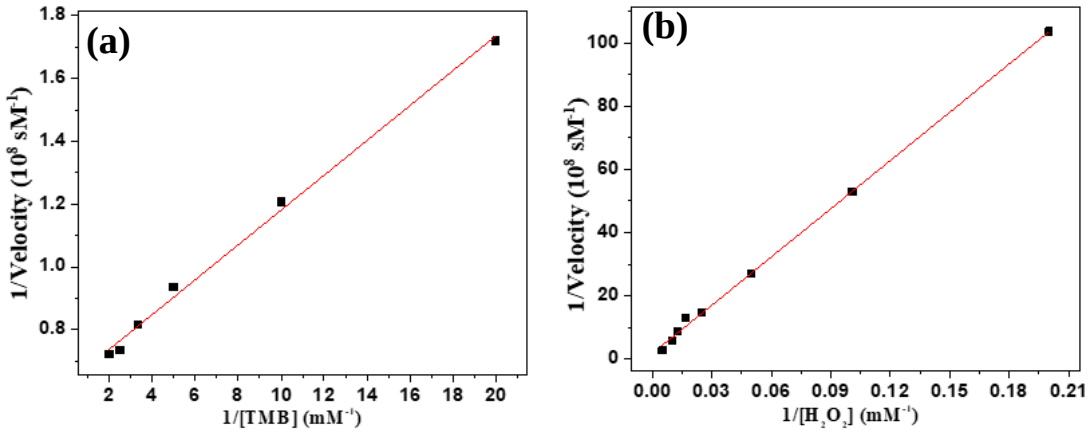


**Fig. S18** Lineweaver-Burk double reciprocal plots for $SiO_2$@$MnCo_2O_4$-1 core-shell nanorattles corresponding to variation of concentration of substrates: (a) TMB and (b) $H_2O_2$.

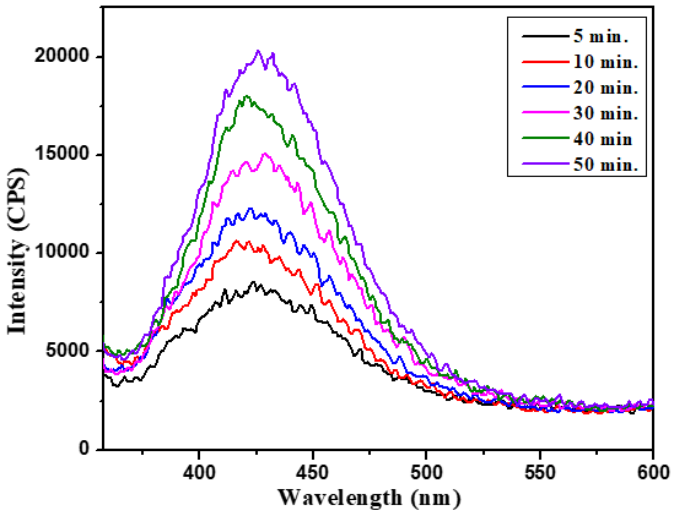


**Fig. S19** Fluorescence spectra indicating the formation of hydroxyl radicals during the catalytic oxidation of TMB by $SiO_2$@$MnCo_2O_4$-1 core-shell nanorattles ($\lambda_{exc}$ = 315 nm).

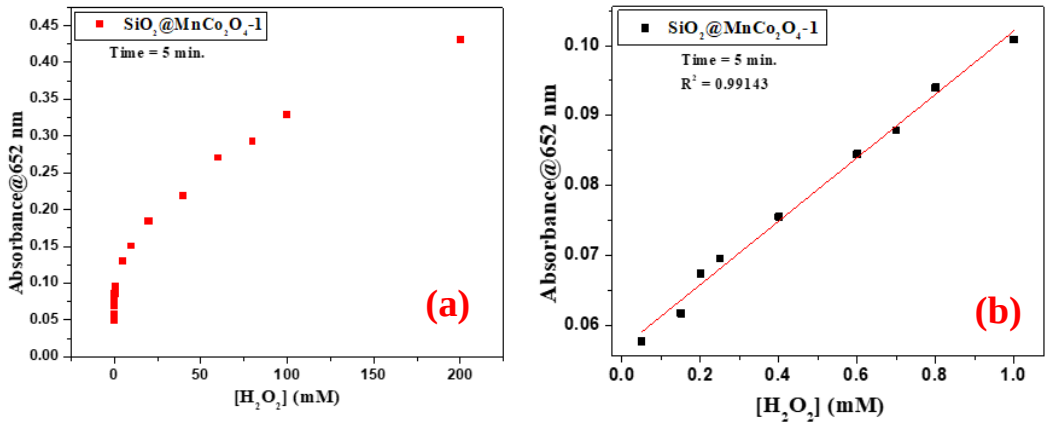


**Fig. S20** (a) Calibration plot for the detection of $H_2O_2$ using $SiO_2$@$MnCo_2O_4$-1 core-shell nanorattles, and (b) calibration plot in the linear range from 0.05 mM to 1.0 mM.

**Table S1** Assignment of IR bands ($cm^{-1}$) of MnCo-LDH and $SiO_2$@MnCo-LDH samples.

| $SiO_2$ | MnCo-LDH | $SiO_2$@MnCo-0.25 | $SiO_2$@MnCo-0.5 | $SiO_2$@MnCo-1 | Assignment |
|---|---|---|---|---|---|
| 3431 | 3470 | 3436 | 3438 | 3428 | υ-(OH) |
| --- | 2217 | 2235 | 2227 | 2233 | υ-(OCN) |
| 1640 | 1637 | 1634 | 1638 | 1647 | δ-(OH) |
| --- | 1382 | 1390 | 1382 | 1388 | υ-(N-O) |
| 1100 | --- | 1105 | 1107 | 1109 | $\upsilon_{asym}$-(Si-O-Si) |
| --- | 1026 | 1024 | 1025 | 1023 | ρ-(OH) |
| 958 | --- | --- | --- | --- | $\upsilon_{sym}$-(Si-OH) |
| 795 | --- | --- | --- | --- | $\upsilon_{sym}$-(Si-O-Si) |
| --- | 639 | 657 | 649 | 659 | υ-(M-OH), M = Mn, Co |
| 469 | --- | 474 | 476 | 468 | δ-(Si-O-Si) |

**Table S2** Summary of TGA results of MnCo-LDH and $SiO_2$@MnCo-LDH samples.

| MnCo-LDH | | $SiO_2$@MnCo-0.25 | | $SiO_2$@MnCo-0.5 | | $SiO_2$@MnCo-1 | | Comment |
|---|---|---|---|---|---|---|---|---|
| Temp. (°C) | % wt. loss | Temp. (°C) | % wt. loss | Temp. (°C) | % wt. loss | Temp. (°C) | % wt. loss | |
| 30-145 | 4.7 | 30-160 | 7.0 | 30-100 | 8.0 | 30-150 | 4.2 | Loss of physisorbed water molecules |
| 145-350 | 17.7 | 160-350 | 3.4 | 100-350 | 5.2 | 150-350 | 12.8 | Loss of intercalated anions from the LDH |
| 350-550 | 6.1 | 350-600 | 5.2 | 350-600 | 3.2 | 350-600 | 6.2 | Dehydroxylation of LDH layers |
| Total | 28.5 | ---- | 15.6 | --- | 16.4 | --- | 23.2 | --- |

**Table S3** EDX analysis results of $SiO_2$@MnCo-LDH samples. The analysis was carried out at three different spots for each sample.

| Sample code | Element | | | | |
|---|---|---|---|---|---|
| | O | | Si | Mn | Co |
| $SiO_2$@MnCo-LDH-0.25 | Wt. % | 39.92 | 29.43 | 10.01 | 20.65 |
| | At. % | 61.30 | 25.74 | 4.69 | 8.27 |
| | Wt. % | 40.21 | 29.23 | 10.02 | 20.54 |
| | At. % | 61.64 | 24.17 | 4.70 | 8.49 |
| | Wt. % | 41.65 | 29.26 | 9.44 | 19.64 |
| | At. % | 60.69 | 24.83 | 4.85 | 9.62 |
| $SiO_2$@MnCo-LDH-0.5 | Wt. % | 41.94 | 23.28 | 11.41 | 23.37 |
| | At. % | 62.8 | 20.80 | 5.41 | 10.99 |
| | Wt. % | 42.09 | 24.77 | 11.06 | 22.08 |
| | At. % | 62.09 | 20.27 | 5.86 | 11.78 |
| | Wt. % | 43.34 | 23.61 | 11.58 | 21.48 |
| | At. % | 62.86 | 21.56 | 5.52 | 10.06 |
| $SiO_2$@MnCo-LDH-1 | Wt. % | 40.38 | 22.53 | 12.77 | 24.32 |
| | At. % | 60.75 | 19.16 | 7.2 | 12.88 |
| | Wt. % | 42.41 | 23.42 | 12.39 | 24.78 |
| | At. % | 61.49 | 19.83 | 7.21 | 11.47 |
| | Wt. % | 41.41 | 23.42 | 11.39 | 23.78 |
| | At. % | 60.49 | 19.83 | 7.47 | 12.21 |

**Table S4** EDX analysis results of $SiO_2@MnCo_2O_4$ nanorattles. The analysis was carried out at three different spots for each sample.

| Sample code | Element | | | | |
|---|---|---|---|---|---|
| | | O | Si | Mn | Co |
| $SiO_2@MnCo_2O_4$-0.25 | Wt. % | 37.38 | 31.18 | 10.72 | 20.72 |
| | At. % | 58.84 | 25.06 | 5.54 | 10.56 |
| | Wt. % | 37.49 | 31.53 | 10.50 | 20.48 |
| | At. % | 59.42 | 25.75 | 5.00 | 9.82 |
| | Wt. % | 36.02 | 31.89 | 11.57 | 20.52 |
| | At. % | 58.48 | 24.87 | 6.53 | 10.13 |
| $SiO_2@MnCo_2O_4$-0.5 | Wt. % | 38.43 | 26.79 | 12.42 | 22.37 |
| | At. % | 58.82 | 24.15 | 6.11 | 12.91 |
| | Wt. % | 39.67 | 27.46 | 11.46 | 22.42 |
| | At. % | 60.38 | 23.80 | 6.09 | 12.73 |
| | Wt. % | 40.14 | 27.40 | 11.79 | 23.66 |
| | At. % | 59.08 | 24.14 | 6.16 | 11.98 |
| $SiO_2@MnCo_2O_4$-1 | Wt. % | 36.22 | 22.45 | 13.77 | 27.55 |
| | At. % | 56.07 | 21.21 | 7.82 | 14.90 |
| | Wt. % | 34.70 | 23.10 | 13.73 | 28.47 |
| | At. % | 56.43 | 21.16 | 7.83 | 14.59 |
| | Wt. % | 36.31 | 22.03 | 14.19 | 27.48 |
| | At. % | 57.51 | 20.97 | 7.49 | 14.03 |

**References:**


1 F. Song and X. Hu, *J. Am. Chem. Soc.*, 2014, **136**, 16481–16484.

2 S. Kandula and P. Jeevanandam, *RSC Adv.*, 2015, **5**, 5295–5306.

3 S. Kandula and P. Jeevanandam, *Eur. J. Inorg. Chem.*, 2015, **2015**, 4260–4274.